CHAPTER II

Synthesis, Crystal Structure and Magnetic Properties of Dimeric Mn^{III} Schiff Base Complexes Including Pseudohalide Ligands. Ferromagnetic Interactions through Phenoxo Bridges and Single Molecule Magnetism

2.1. Introduction

Schiff base complexes of Mn^{III}, though well known, continue to generate interest due to their potential applications in fields as diverse as homogeneous catalysis and magnetic materials.[1] Complexes of general formula Mn(SB)X, where SB is a tetra-dentate Schiff base and X is usually an anionic ligand, often crystallize as phenoxo-bridged dimers which may exhibit a range of magnetic interactions depending upon the bridge geometry.[2-19] Some of these complexes have been investigated in detail for their SMM (single molecule magnet) properties.[6,19] Magnetic properties of one dimensional chains formed by bridging ligands (for example, azide[20]) and more recently, coordination networks resulting from second coordination sphere interactions[21] have also been reported. In this chapter, three new phenoxo-bridged complexes, Mn(salpn)NCO (**1**), Mn(salmen)N_3 (**2**), and Mn(acphpn)N_3 (**3**) crystallographic structure determination, spectral and variable temperature magnetic studies discussed in detail. The Schiff bases involved are depicted in Scheme 1.4. Even though these new complexes do not greatly enlarge in the of bridging geometries already reported for this class of compounds, they do not

demonstrate the role of intermolecular interactions in causing dramatic differences between otherwise similar magnetically coupled systems. In particular, compound **1**, unlike any other previously reported phenoxo-bridged Mn(III,III) system remains ferromagnetic in the entire temperature rang 2 – 300 K with a high spin (S = 4) ground state.

2.2. Experimental Section

2.2.1. Synthesis

All chemicals used for synthesis were reagent grade. The Schiff bases were formed *in situ* in the presence of the appropriate metal salt. **Caution:** Azide compounds are potentially explosive and should be prepared only in small quantities and handled with care.

[Mn(salpn)NCO]$_2$ (1): In a beaker open to the atmosphere, salicylaldehyde (0.244 g, 1.00 mmol) and 1,3-diaminopropane (0.071 g, 1.0 mmol) were stirred in 40 mL of ethanol. $Mn(CH_3COO)_2.4H_2O$ (0.245 g, 1.00 mmol) was added, and stirring was continued for about 1 h. To the resulting solution, NaOCN (0.130 g, 2.00 mmol) dissolved in a minimum amount of water was added, stirring continued for 3 h, to complete the aerial oxidation of Mn^{II}. The filtered solution was kept in a refrigerator (5º C) for one week when dark green crystals deposited. Yield: 0.234 g (0.62 mmol, 62%). Anal. Calcd. for $C_{18}H_{16}N_3O_3Mn$: C, 57.1; H, 4.27; N, 11.14. Found: C, 57.20; H, 4.23; N, 11.23. Characteristic IR absorptions (cm^{-1}): ν_a(NCO) 2160, ν_s(NCO) 1313, δ(NCO) 615, $\nu_{schiff\ base}$(C=N) 1620.

$[Mn(salmen)N_3]_2$ (2): In a beaker open to the atmosphere, salicylaldehyde (0.244 g, 1.00 mmol) and 1,2-diaminopropane (0.074 g, 1.0 mmol) were stirred in 40 mL of methanol. $Mn(CH_3COO)_2.4H_2O$ (0.245 g, 1.00 mmol) was added, and stirring was continued for about 1 h. To the resulting solution, NaN_3 (0.130 g, 2.00 mmol) dissolved in a minimum amount of water was added and stirring continued for 3 h to complete the aerial oxidation of Mn^{II}. The resulting microcrystalline precipitate was filtered off and dried. Yield: 0.306 g (0.81 mmol, 81%). It was recrystallized by slow evaporation of an acetonitrile solution at room temperature yielding dark-brown X-ray quality crystals. Anal. Calcd. for $C_{18}H_{16}N_5O_2Mn$: C, 54.12; H, 4.27; N, 18.57. Found: C, 54.19; H, 4.32; N, 18.98. Characteristic IR absorptions (cm^{-1}): $\nu_a(N_3)$ 2035, $\nu_s(N_3)$ 1309, $\delta(N_3)$ 599, $\nu_{schiff\ base}(C=N)$ 1612.

$[Mn(acphpn)N_3]_2$ (3): In a beaker open to the atmosphere, $Mn(CH_3COO)_2.4H_2O$ (0.245 g, 1.00 mmol) and NaN_3 (0.130 g, 2.00 g) were dissolved in 30 mL methanol and filtered. 2-Hydroxyacetophenone (0.272 g, 2.00 mmol) and 1, 3-diaminopropane (0.071 g, 1.0 mmol) were dissolved in 30 mL methanol and filtered. The two solutions were mixed and stirred for 2h to complete the aerial oxidation of Mn^{II}. The filtered solution was kept at room temperature for three days to obtain dark green crystals. Yield: 0.254 g (0.63 mmol, 63%). Anal. Calcd. for $C_{19}H_{20}N_5O_2Mn$: C, 56.25; H, 4.98; N, 17.26. Found: C, 56.45; H, 4.98; N, 17.36. Characteristic IR absorptions (cm^{-1}): $\nu_a(N_3)$ 2038, $\nu_s(N_3)$ 1300, $\delta(N_3)$ 522, $\nu_{schiff\ base}(C=N)$ 1587.

2.2.2. Physical Measurements

IR spectra were obtained in KBr pellets using Shimadzu FT-IR 8000 spectrometer. Elemental analysis of the complexes was performed on a FLASH EA SERIES CHNS analyzer. Absorption spectra for **1-3** in methanol were measured on a Shimadzu UV-3100 PC spectrometer. The magnetic susceptibility was measured in the 1.98-300 K temperature range using a Quantum Design MPMS SQUID susceptometer. The samples were pressed into pellets to avoid orientation effects of the microcrystals during magnetic measurements. Diamagnetic corrections were applied using Pascal's constants.[22] The magnetic susceptibilities have been computed both with the program SUSCEP[23] based on the expression derived from the isotropic spin-exchange Hamiltonian $\hat{H} = -2J\hat{S}_1\hat{S}_2$ ($S_1 = S_2 = 2$) and van Vleck's equation,[24] and by exact calculations of the energy levels associated to the spin Hamiltonian through diagonalization of the full matrix with a general program for axial symmetry.[25] In the latter case, least-squares fittings were accomplished with an adapted version of the function-minimization program MINUIT.[26]

2.2.3. X-ray Crystallography

X-ray data were collected for compounds **1-3** on a Bruker SMART APEX CCD X-ray diffractometer, using graphite-monochromated Mo-Kα radiation (λ = 0.71073 Å). Data were reduced using SAINTPLUS,[27] and a multi-scan absorption correction using SADABS[28] was performed. The structures were solved using SHELXS-97 and full matrix least squares refinements against F^2 were carried out using SHELXL-97.[29] All ring hydrogen atoms were assigned on the basis of

Table 2.1 Crystallographic data and structure refinement for **1**, **2** and **3**

	1	**2**	**3**
Formula	$C_{36}H_{32}Mn_2N_6O_6$	$C_{34}H_{32}Mn_2N_{10}O_4$	$C_{38}H_{40}Mn_2N_{10}O_4$
Formula weight	754.56	754.58	810.68
Crystal system	monoclinic	monoclinic	monoclinic
a (Å)	8.6269(5)	8.6770(17)	8.4760(5)
b (Å)	13.6701(8)	13.731(3)	20.2098(12)
c (Å)	14.3355(8)	14.326(3)	10.3259(6)
α (º)	90	90	90
β (º)	105.1050(10)	104.316(3)	91.2810(10)
γ (º)	90	90	90
V (Å^3)	1632.18(16)	1653.8(6)	1768.37(18)
Space group	$P\,2_1/n$	$P\,2_1/n$	$P\,2_1/n$
Z	2	2	2
T (K)	100(2)	298(2)	298(2)
ρ_{calcd} (g cm^{-3})	1.535	1.515	1.522
μ (mm^{-1})	0.832	0.820	0.772
θ Range (º)	2.09 - 28.26	2.09 - 28.31	2.02 - 28.24
h/*k*/*l* indices	-11, 11/ -18,18/ -18, 19	–11, 11/ –17, 18/ –18, 18	–11,11/ –26, 26/ –13, 13
Reflections collected	18686	18714	20250
Unique reflection, R_{int}	4047, 0.0218	3969, 0.0536	4221, 0.0280
GooF	1.363	1.058	1.028
$R_1[I > 2\sigma(I)]$	0.0351	0.0616	0.0360
wR_2 [all data]	0.0986	0.1361	0.0916
$\Delta\rho_{max}$, $\Delta\rho_{min}$ (e.Å^{-3})	0.328, -0.223		
Weight. scheme (A, B)	0.0518, 0.46	0.0702, 0.58	0.0588, 0.29

geometrical considerations and were allowed to ride upon the respective carbon atoms. All hydrogen atoms were assigned fixed U_{iso} values, equal to $1.2U_{eq}$ of the parent atom for ring and $1.5U_{eq}$ for methyl hydrogens. Crystallographic data and structure refinement parameters are presented in Table 2.1.

2.3. Results and Discussion

2.3.1. Crystal Structures

All three complexes crystallize in the $P2_1/n$ space group. Complexes **1** and **2** have almost identical formula weights and nearly equal unit cell dimensions, even though their chemical compositions are different. The crystals of all three complexes contain dinuclear Mn^{III} entities (Figure 2.1), wherein the two centrosymmetrically related five-coordinate metal centers are held by two weak phenoxo bridges (Mn···O in the 2.49-2.59 Å range). Within each five-coordinate unit, the tetradentate Schiff base ligand chelates in the equatorial mode, while the axial position is occupied by a nitrogen atom from the pseudo-halide ion, azide or cyanate, coordinating in a bent mode. The equatorial donor atoms (O_2N_2) are very nearly coplanar even though the manganese atom deviates significantly from this plane (0.16 Å in **1**; 0.20 Å in **2**; 0.13 Å in **3**). The mean planes of the two halves of the Schiff base ligands (excluding the methylene groups) are inclined with respect to each other by 15º in the three crystals. There are only slight differences in the Mn–(N,O) distances in the three complexes: Mn–O(*eq*.)$_{av}$, Mn–N(*eq*.)$_{av}$, Mn–N(*ax*.) are respectively, 1.90, 2.01, 2.14 Å in **1**; 1.88, 1.99, 2.14 Å in **2**; 1.89, 2.01, 2.17 Å in **3**. The overall coordination geometry of each

Mn^{III} ion is thus distorted octahedral with the Jahn-Teller elongation along the NCO/NNN–Mn...O axis.

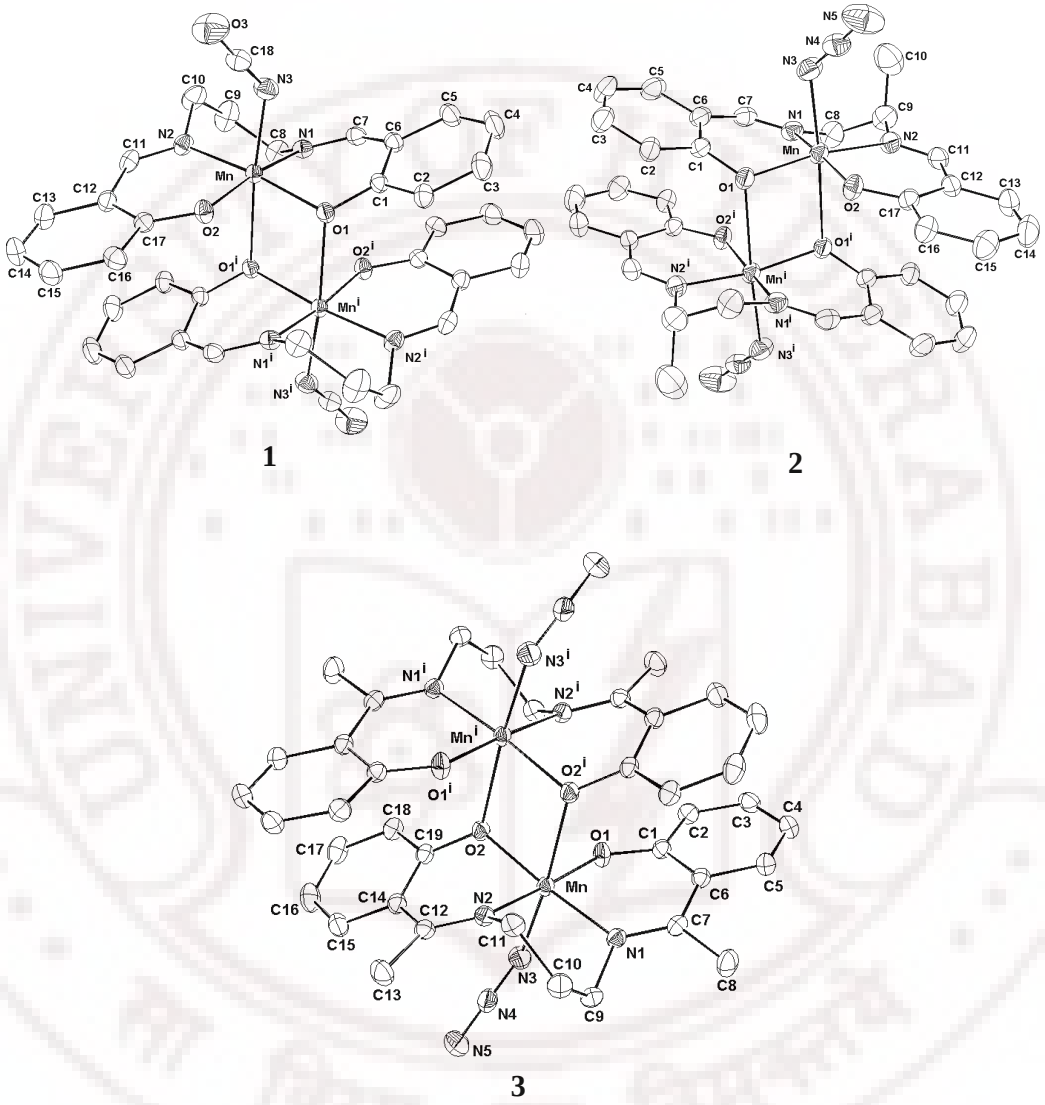

Figure 2.1 ORTEP view of the dimers in $[Mn(salpn)NCO]_2$ (**1**) $[Mn(salmen)N_3]_2$ (**2**) $[Mn(acphpn)N_3]_2$ (**3**). Hydrogen atoms are omitted, and the thermal ellipsoids are represented at the 30% probability level.
i = $–x$+1,$–y$+1,$–z$+1 for **1**; $–x$+1,$–y$+1,$–z$+1 for **2**; $–x$,$–y$+2,$–z$ for **3**.

Table 2.2 Selected bond lengths [Å] and angles [°] for $[Mn(salpn)NCO]_2$ (**1**)

Mn-O1	1.9162(11)	Mn-N1	2.0261(13)	Mn-N3	2.1394(15)
Mn-O2	1.8757(11)	Mn-N2	1.9920(13)	Mn-O1#1	2.5130(11)
N3-C18	1.169(2)	C18-O3	1.195(2)		
O1-Mn-N1	87.73(5)	O2-Mn-N1	169.90(5)	O1-Mn-O1#1	79.42(4)
O1-Mn-N2	170.78(5)	O2-Mn-N2	90.58(5)	O2-Mn-O1#1	86.42(4)
O1-Mn-N3	96.07(6)	O2-Mn-N3	95.82(6)	N1-Mn-O1#1	83.50(5)
N1-Mn-N3	94.29(6)	O2-Mn-O1	91.07(5)	N2-Mn-O1#1	91.63(5)
Mn-N3-C18	135.11(14)	N2-Mn-N1	89.06(6)	N3-Mn-O1#1	175.02(5)
N3-C18-O3	178.2(2)	Mn-O1-Mn#1	100.58(4)	#1 –*x*+1, –*y*+1, –*z*+1	

Table 2.3 Selected bond lengths [Å] and angles [°] for $[Mn(salmen)N_3]_2$ (**2**)

Mn-O1	1.903(2)	Mn-N1	1.988(3)	Mn-N3	2.137(3)
Mn-O2	1.860(2)	Mn-N2	1.984(3)	Mn-O1#1	2.589(2)
N3-N4	1.183(5)	N4-N5	1.153(5)		
O1-Mn-N1	88.85(11)	O2-Mn-N1	169.18(11)	O1-Mn-O1#1	81.46(9)
O1-Mn-N2	163.55(12)	O2-Mn-N2	92.15(12)	O2-Mn-O1#1	87.61(9)
O1-Mn-N3	96.15(12)	O2-Mn-N3	97.00(13)	N1-Mn-O1#1	82.78(10)
N1-Mn-N3	92.79(13)	O2-Mn-O1	94.65(10)	N2-Mn-O1#1	83.87(10)
Mn-N3-N4	127.8(3)	N2-Mn-N1	81.93(13)	N3-Mn-O1#1	174.99(11)
N3-N4-N5	177.9(5)	Mn-O1-Mn#1	98.55(4)	#1 –*x*+1, –*y*+1, –*z*+1	

Table 2.4 Selected bond lengths [Å] and angles [°] for $[Mn(acphpn)N_3]_2$ (**3**)

Mn-O1	1.8633(12)	Mn-N1	2.0148(13)	Mn-N3	2.1722(16)
Mn-O2	1.9124(11)	Mn-N2	2.0050(13)	Mn-O2#1	2.4929(12)
N3-N4	1.177(2)	N4-N5	1.157(3)		
O1-Mn-N1	89.51(5)	O2-Mn-N1	169.78(5)	O2-Mn-O2#1	78.77(5)
O1-Mn-N2	174.51(6)	O2-Mn-N2	85.63(5)	O1-Mn-O2#1	88.00(5)
O1-Mn-N3	91.59(6)	O2-Mn-N3	95.91(6)	N1-Mn-O2#1	91.84(5)
N1-Mn-N3	93.52(6)	O1-Mn-O2	94.16(5)	N2-Mn-O2#1	86.58(5)
Mn-N3-N4	130.80(14)	N2-Mn-N1	89.82(6)	N3-Mn-O2#1	174.61(5)
N3-N4-N5	178.5(2)	Mn-O2-Mn#1	101.23(5)	#1 –*x*, –*y*+2, –*z*	

Coming to the dimer formed by bridging the five-coordinate complex molecules, the plane of the Mn_2O_2 bridge is nearly perpendicular to the equatorial coordination plane: dihedral angle, 88.5º in **1**, 87.4º in **2**, 89.7º in **3**. The axial N atom deviates only slightly from the bridging plane (0.08 Å in **1**; 0.16 Å in **2**; 0.03 Å in **3**). The most important difference between the three dimers arises from the bridging bond lengths (Å) and angles (º): Mn–O, Mn···O, Mn–O···Mn are respectively, 1.92, 2.51, 100.6 in **1**; 1.90, 2.59, 98.5 in **2**; 1.91, 2.49, 101.2 in **3**. The Mn···Mn distance in the three dimers is 3.43 Å. In summary, the bridge geometry in compound **3** is characterized by a shorter Mn···O distance coupled with a wider Mn–O···Mn angle while the longer Mn···O* distance goes with a more acute Mn–O···Mn angle in compound **2**; compound **1** has a bridge geometry intermediate between those of **2** and **3**. These differences have an important bearing on the magnetic properties. Selected bond distances and angles are collated in Tables 2.2-2.4.

2.3.2. Spectral Studies

2.3.2a. FTIR Spectra

The IR spectra of compound **1** exhibits strong absorption in the range of 2100-2200 cm^{-1}, which is attributed to the asymmetric stretching vibration of N-bonded cyanate group. Compounds 2 and **3** exhibit strong absorption in the range of 2030-2040 cm^{-1}, which is attributed to the asymmetric stretching vibration of N-bonded azide group. All three compounds exhibit strong absorption at 1590-1630 cm^{-1}, which is assignable to the (-C=N) stretching vibration of Schiff-base. All these absorptions are with in the reported range.[30]

2.3.2b. Electronic Spectra

In all three complexes, the Mn^{III} (d^4) is a high-spin ion, and it has distorted octahedral geometry. For pure octahedral d^4 (^5D ground state term) system, only one electronic absorption ($^5T_{2g} \leftarrow {}^5E_g$) is possible, due to distorted octahedral geometry the complexes **1-3** have four broad absorption bands. The solution spectra of the compounds **1-3** were measured in methanol (Figure 2.2). The low intensity absorption bands in the range 18.23, 351 for complex **1**, 16.07, 322 for complex **2**

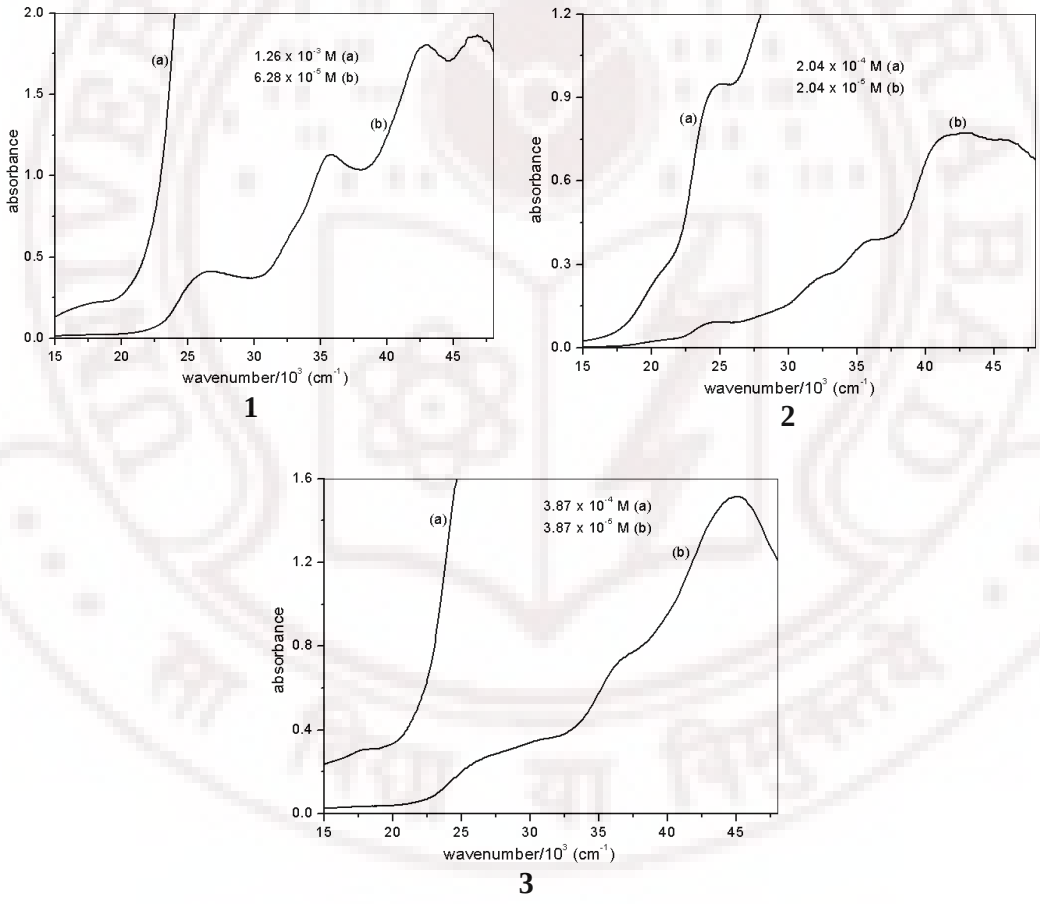

Figure 2.2 Electronic absorbance spectra of complex **1**, **2** and **3** in methanol.

and 18.93, 819 for complex **3** ($\bar{\nu}_{max}$ /10^3cm^{-1}, ε_{max}/cm^{-1}M^{-1}) respectively, which are assigned to d-d transition. The high intensity absorption bands in the range 26.72, 6487; 35.64, 17818; 42.73, 28614 for complex **1,** 24.27, 4637; 28.55, 6147; 32.22, 12230; 42.82, 38294 for complex **2**, and 26.77, 6899; 32.32, 9767; 45.12, 39069 for complex **3** ($\bar{\nu}_{max}$ /10^3cm^{-1}, ε_{max}/cm^{-1}M^{-1}) respectively, which are assigned to intraligand π-π* transitions in the complexes, the low intensity d-d transitions were masked in this range.

2.3.3. Magnetic Measurements

The variations of the molar magnetic susceptibility χ_m, and of the product $\chi_m T$ in the temperature range 1.98-300 K for the three complexes are shown in Figure 2.3. The room temperature $\chi_m T$ values (cm^3 mol^{-1} K) are nearly equal for the three dimers and comparable to the expected spin-only value of 6.00 cm^3 mol^{-1} K per dinuclear Mn^{III} unit: 6.19 for **1**; 5.99 for **2**; 5.90 for **3**. However, the three compounds behave differently when the temperature is lowered. In the case of compound **1**, $\chi_m T$ increases continuously to reach a value of 10.01 cm^3 mol^{-1} K at 1.98 K. Since the expected value for the S = 4 ground state is 10.00 cm^3 mol^{-1} K, the above result proves the ferromagnetic coupling within the dimer and the absence of significant competing effects from Mn^{III} single ion zero-field splitting and/or antiferromagnetic inter-dimer interactions. Compound **2** also shows an increase upon lowering the temperature. However a maximum $\chi_m T$ of 7.85 cm^3 mol^{-1} K is reached at 5.82 K. Further cooling leads to a rapid decrease to 6.34 cm^3 mol^{-1} K at 2 K. Therefore, while the intra-dimer interaction in compound **2** is ferromagnetic like in **1**, there are

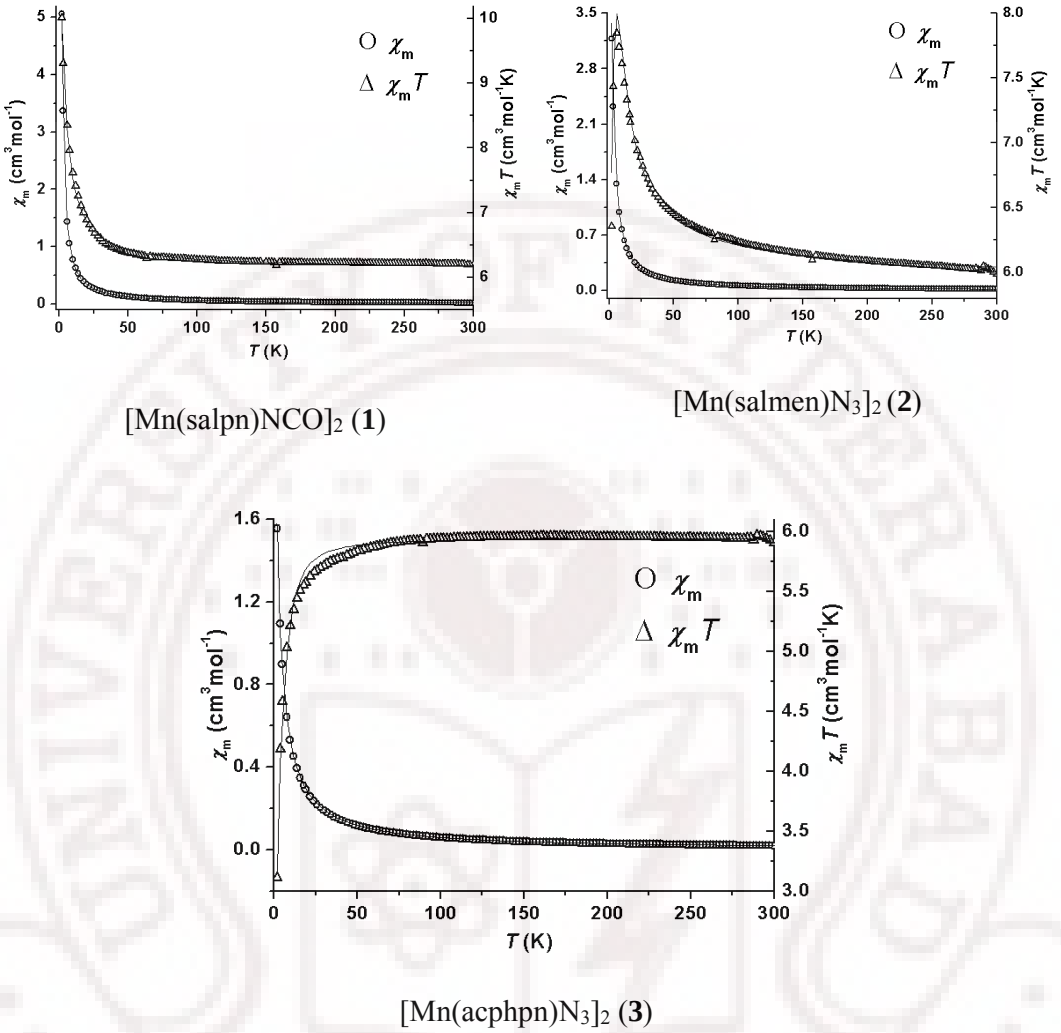

Figure 2.3. Temperature variation of the magnetic susceptibility χ_m and $\chi_m T$ product (per dimeric unit) for compounds **1** – **3**. Magnetic field strength used: 1000 Oe (**1**); 5000 Oe (**2**); 3000 Oe (**3**).

competing Mn^{III} single ion zero-field splitting (zfs) effects and/or antiferromagnetic inter-dimer interactions leading to a rapid fall in $\chi_m T$ below 6 K. In sharp contrast to **1** and **2**, compound **3** is clearly an antiferromagnetically coupled dimer with the $\chi_m T$

value decreasing continuously upon cooling from room temperature to reach a value of 3.11 cm^3 mol^{-1} K at 2 K.

The magnetic susceptibilities were therefore computed through exact diagonalisation of the spin Hamiltonian including Zeeman and zfs terms and isotropic exchange[25] and fitted to the experimental magnetic data by least-squares techniques.[26] The calculations employed the Hamiltonian, $\beta H \cdot g \cdot (S_1 + S_2) - 2JS_1 \cdot S_2 + D(S_{z1}^2 + S_{z2}^2)$. Although *g*-tensor was assumed to be axial, the difference between its parallel and perpendicular components was not significant. The single ion zero-field splitting parameter, *D* is identical for the two centrosymmetrically related Mn^{III} ions in the dimer. The best sets of parameters obtained by least square fitting were: **1**, J = 0. 42(2) cm^{-1}, D = 0.0006(2) cm^{-1}, g = 2.022(1), LSE (least squares error) = 0.00007; **2**, J = 0.58(1) cm^{-1}, D = – 2.32(4) cm^{-1}, g = 2.000(3), LSE = 0.0001; **3**, J = – 0.20(2) cm^{-1}, D = – 0.009(3) cm^{-1}, g = 1.997(2), LSE = 0.00003. The solid lines in the Figure 2.3 were computed using the above parameters. The differences between the three compounds are further illustrated in Figure 2.4, by plotting together their effective magnetic moments as a function of temperature. While the differences in *J* values are in agreement with the differences in bridge geometry in the molecular structures of **1**-**3**, the large zfs difference between **1** and **3** on the one hand, and **2** on the other hand, is difficult to explain in view of their very similar coordination geometries. This apparent discrepancy suggests that Mn^{III} zfs may not be the unique effect competing with the isotropic spin-spin interactions, but that possibly inter-dimer magnetic interactions also operate in these complexes. As a first step to check this hypothesis, we also

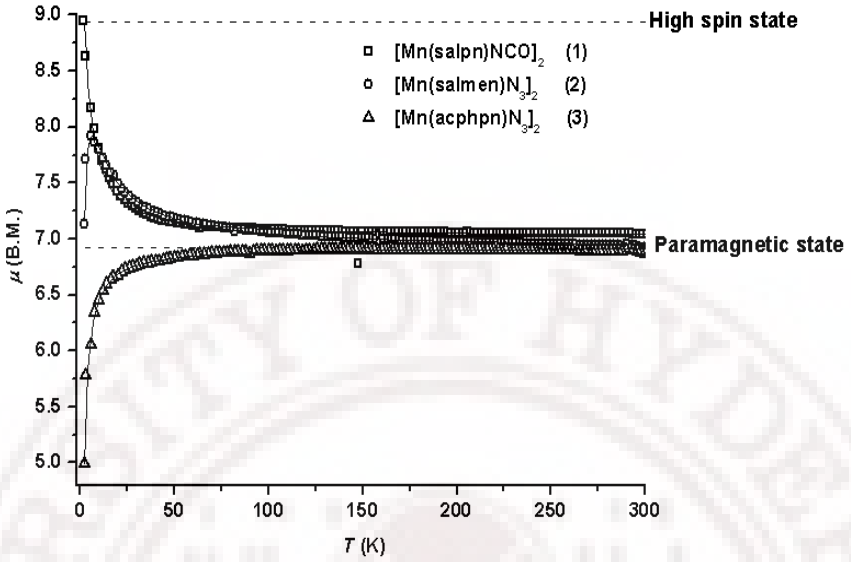

Figure 2.4. Temperature variation of magnetic moment (μ_{eff} per dimeric unit) for the three compounds (**1**, **2** and **3**)

computed the magnetic susceptibilities using the dimer model[24] including inter-dimer interactions within the molecular field approximation.[31] The best sets of parameters obtained by least square fitting were : **1**, J = 0.364(6) cm^{-1}, zj = 0.0020(3) cm^{-1}, g = 2.025(fixed), LSE = 0.002; **2**, J = 0.853(9) cm^{-1}, zj = – 0.0576(2) cm^{-1}, g = 1.99(fixed), LSE = 0.001; **3**, J = – 0.1385 (5) cm^{-1}, zj = – 0.0561 (5) cm^{-1}, g = 2.00(fixed), LSE = 0.0004. The quality of the fits, although satisfactory, was not as good as the previous ones, suggesting the operation of both Mn^{III} zfs and antiferromagnetic inter-dimer interactions, at least for **2** and **3**. As a further step, we also computed the magnetic susceptibilities through exact diagonalisation of the spin Hamiltonian including axial Zeeman and zfs terms, isotropic exchange, and inter-dimer interactions within the molecular field approximation. Although the quality of the fits was excellent, D and zj were correlated preventing us to safely estimate

independently the respective contribution of these two factors to the magnetic susceptibilities in this series of dimeric Mn^{III} compounds. Considering the similar Jahn-Teller elongation in complexes **1-3** the *D* is expected to be similar and negative in all the three compounds. Therefore, based on the observed temperature dependence of the magnetic moments and the fitting results, it is reasonable to conclude that the magnitude of *D* is very small for these compounds so that the variation of the magnetic moment at low temperatures is dominated by inter-dimer interactions.

It is worthwhile to examine the reason for the conspicuous difference in the inter-dimer interactions in compounds **1** and **2**. The intermolecular interactions between dimers are shown in Figure 2.5. The shortest Mn···Mn separation between dimers is nearly the same in both compounds: 8.86 Å in **1** and 8.68 Å in **2**. A close examination of the crystal packing shows that the important inter-dimer interactions present in both compounds are (i) =CH···N_c (2.52 Å in **1**; 2.47 Å in **2**), (ii) =CH···O_t / N_t (2.62 Å in **1**; 2.57 Å in **2**) and (iii) Ph-H···Cπ (2.83 Å in **1**; 2.66 Å in **2**) where, suffixes *c* and *t* refer to coordinated and terminal atom of the pseudohalide ion. The only difference between the two compounds is the presence of a π-stacking interaction (3.36 Å)[32] in **1** while such an interaction is blocked in **2** by the methyl group. Instead, a hydrogen atom of the methyl group in **2** is involved in a C-H···Phπ interaction (2.88 Å).[33] The above two contacts which distinguish the packing in the two compounds are shown by red dotted lines in Figure 2.5. Correlation of these observations with the magnetic data seems to suggest that the methyl group

interaction in **2** is responsible for the antiferromagnetic inter-dimer pathway, while the π-stacking in **1** is ferromagnetic and all other contacts common to both

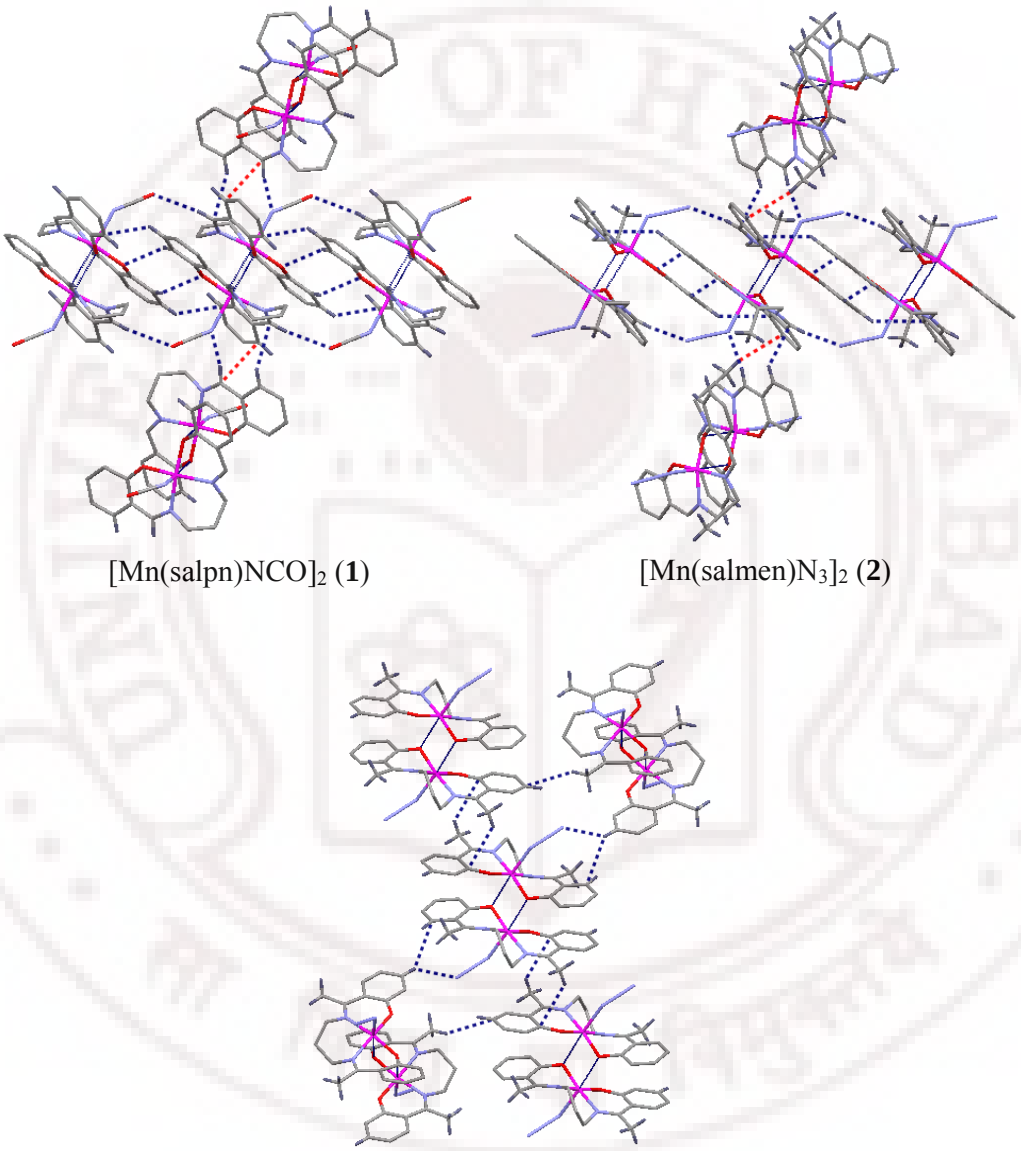

[Mn(salpn)NCO]$_2$ (**1**) [Mn(salmen)N$_3$]$_2$ (**2**)

[Mn(acphpn)N$_3$]$_2$ (**3**)

Figure 2.5. Intermolecular interactions between dimers in complexes **1**, **2** and **3**.

compounds may be of the antiferromagnetic type. This leads to a near-cancellation of the interdimer interactions so that the dimer in **1** remains ferromagnetically coupled down to 2K. The methyl C-H···Phπ interaction is also present in **3** (3.02, 3.13 Å) while the other interactions listed above are absent. The terminal azido in this compound is involved in a Ph-H···N interaction (2.59 Å). As noted above, the interdimer exchange interaction determined by the fitting of magnetic susceptibility is antiferromagnetic in this compound as well. DC-Magnetisation measurements were done for **1** and **2** mainly to check for hysteresis. Attempts to fit the magnetisation data (Figure 2.6) using the parameters previously derived from temperature variation of molar susceptibility gave satisfactory result only for **2**. It seems that a larger anisotropic term (D) will be needed for **1**. The reason for this discrepancy is not evident. The absence of hysteresis indicates that inter-dimer interactions do not lead to long range order in **1** and **2**, above 1.9 K.

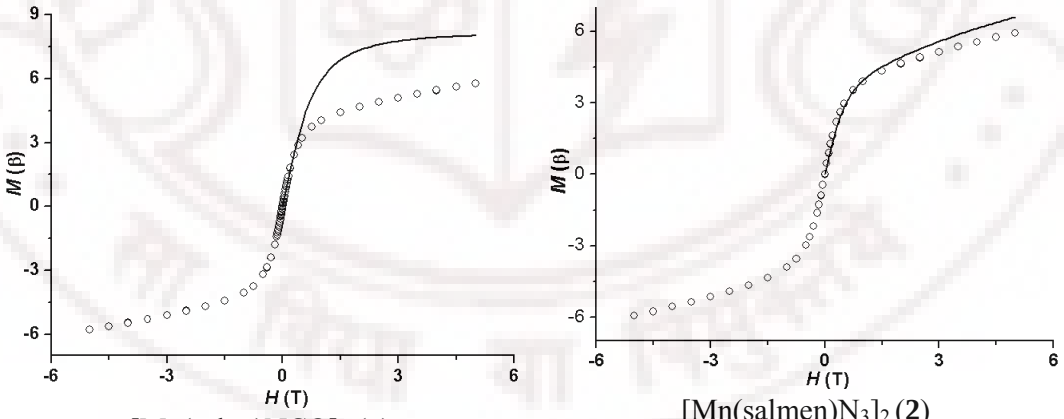

[Mn(salpn)NCO]$_2$ (**1**) [Mn(salmen)N$_3$]$_2$ (**2**)

Figure 2.6. Variation of magnetization with applied field at 2 K for complexes **1** and **2**. The solid lines represent simulations based on the parameters obtained by fitting the temperature dependent molar susceptibility data

A look at the twenty-odd phenoxo bridged dinuclear Mn^{III} compounds (Table 1.1) reported[2–19] to date shows that the exchange splitting, $2J$, falls in the range, –3.4 to 12.6 cm^{-1}, with only two instances of $2J > 4$ cm^{-1}. Further, the small magnitude of the interaction energy may reduce the precision with which it can be determined from least squares analysis when competing influences from zero-field splitting and inter-dimer interactions are present. Therefore, a precise correlation of exchange interactions with molecular structure is difficult to evaluate in this class of compounds. In the case of several dimers having water, thiocyanate or chloride as axial ligands and showing ferromagnetic interaction, it was found that the $2J$ value has a reciprocal correlation with the Mn···O bond distance (2.4-3.7 Å).[5] However, for the present compounds, the relationship is reversed, with the following respective Mn···O distances (Å) and $2J$ (cm^{-1}) values: 2.49, –0.4 (**3**); 2.51, 0.84 (**1**); 2.59, 1.16 (**2**). Because four magnetic orbitals are involved on each centre, it is unlikely that the exchange interaction may be controlled by just one structural parameter. In this respect, it is worth noting that the increase in $2J$ (cm^{-1}) parallels the decrease in Mn–O···Mn angle (º), with the following respective values: – 0.4, 101.2 in **3**; 0.84, 100.6 in **1**; 1.16, 98.5 in **2**.

In order to check whether compounds **1** and **2** behave as single molecule magnets (SMMs), their *ac* susceptibility was measured in the temperature range 2-10 K at two different frequencies (100 and 1000 Hz). The observation of frequency dependent in-phase (χ') and out-of-phase (χ'') magnetic susceptibilities (Figure 2.7) suggests an SMM behavior for both compounds. Even though no maxima were seen in the above data obtained with zero *dc* field, clear maxima appeared when a *dc* field

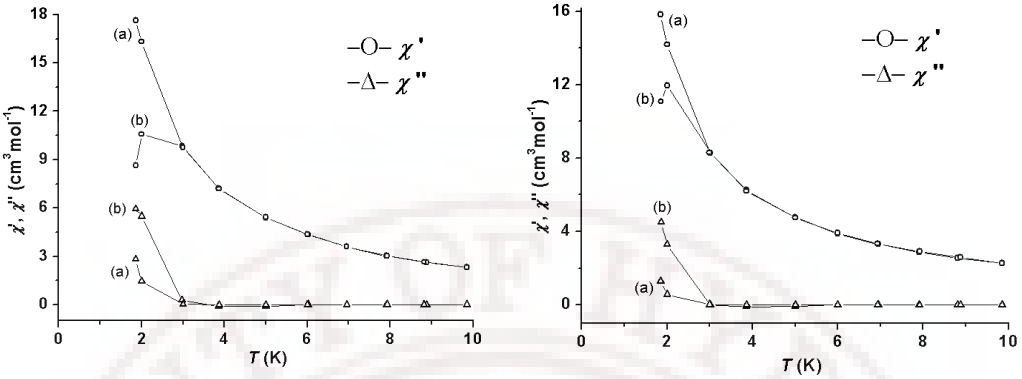

[Mn(salpn)NCO]$_2$ (**1**) [Mn(salmen)N$_3$]$_2$ (**2**)

Figure 2.7. Temperature variation of the in-phase (χ') and out-of-phase (χ'') components of the ac-magnetic susceptibility in zero static field for complexes **1** and **2** at, (a) 100Hz and (b) 1000Hz. Solid lines between the experimental data points are shown as a guide to the eye, they do not result from fitting.

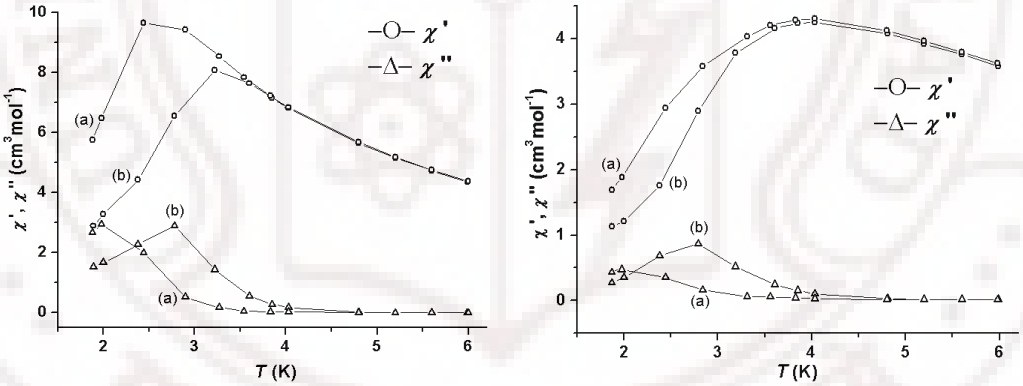

[Mn(salpn)NCO]$_2$ (**1**) [Mn(salmen)N$_3$]$_2$ (**2**)

Figure 2.8. Temperature variation of the in-phase (χ') and out-of-phase (χ'') components of the ac-magnetic susceptibility for complex **1** at a DC field of 0.1 T and for complex **2** at a DC field of 0.5 T. The AC field fluctuates at a frequency of (a) 100Hz and (b) 1000Hz. Solid lines between the experimental data points are shown as a guide to the eye, they do not result from fitting.

(0.1 and 0.5 T for complexes **1** and **2**, respectively) was applied (Figure 2.8). While the above results are in agreement with observation of an SMM behavior for other phenoxo bridged Mn^{III} dimers,[6] further detailed ac susceptibility measurements needed for evaluating the relaxation parameters of complexes **1** and **2** is not attempted in the present study.

2.4. Conclusions

The present results further demonstrate, in line with previous studies,[5,6] that a precise correlation of the magnetic exchange parameter with bridge geometry is difficult in the case of phenoxo-bridged dimers due to the weakness of the magnetic coupling and the involvement of several magnetic orbitals in the interaction. An important finding from the present study is that weak interdimer interactions like stacking or C-H$\cdots\pi$ can cause dramatic changes in the overall temperature dependence of the magnetic susceptibility as seen in the case of compounds **1** and **2**, both of which are ferromagnetically coupled dimers. Alkyl substituents on the Schiff base are effective in modulating the interdimer interactions causing differences in behavior at lower temperatures. The ferromagnetically coupled dimers, in spite of their very small magnitude of the zero field splitting do show evidence for single molecule magnetism.

2.5. References

1. *Review*: Wezenberg, S. J.; Kleij, A. W. *Angew. Chem. Int. Ed.* **2008**, *47*, 2.

2. Shyu, H.; Wei, H.; Wang, Y. *Inorg. Chim. Acta* **1999**, *290*, 8.

3. Karmakar, R.; Choudhury, C. R.; Bravic, G.; Sutter, J.-P.; Mitra, S. *Polyhedron* **2004**, *23*, 949.

4. Lecren, L.; Wernsdorfer, W.; Li, Y.-G.; Vindigi, A.; Miyasaka, H.; Clerac, R. *J. Am. Chem. Soc*. **2007**, *129*, 5045.

5. Miyasaka, H.; Clerac, R.; Ishii, T.; Chang, H.; Kitagawa, S.; Yamashita, M. *J. Chem. Soc., Dalton Trans*. **2002**, 1528.

6. Lu, Z.; Yuan, M.; Pan, F.; Gao, S.; Zhang, D.; Zhu, D. *Inorg. Chem.* **2006**, *45*, 3538.

7. Ko, H. H.; Lim, J. H.; Kim, H. C.; Hong, C. S. *Inorg. Chem*. **2006**, *45*, 8847.

8. Saha, S.; Mal, D.; Koner, S.; Bhattacherjee, A.; Gutlich, P.; Mondel, S.; Mukherjee, M.; Okamoto, K.-I. *Polyhedron*, **2004**, *23*, 1811.

9. Matsumoto, N.; Zhong, Z.; Okawa, H.; Kida, S. *Inorg. Chim. Acta* **1989**, *160*, 153.

10. Bermejo, M. R.; Castineiras, A.; Garcia-Montergudo, J. C.; Rey, M.; Sousa, A.; Watkinson, M.; McAuliffe, C. A.; Pritchard, R. G.; Beddose. R. I. *J. Chem, Soc., Dalton Trans.* **1996**. 2935.

11. Garcia-Deibe, A.; Sousa, A.; Bermejo, M. R.; MacRory, P. P.; McAuliffe, C. A.; Pritchard, R. G.; Hellowell, M. *J. Chem. Soc., Chem. Commun*. **1991**, 728.

12. (*a*) Mikuriya, M.; Yamato, Y.; Tokii, T. *Bull. Chem. Soc. Jpn*. **1992**, *65*, 1466. (*b*) Kennedy, B. J.; Murray, K. *Inorg. Chem*. **1985**, *24*, 152.

13. Sailaja, S.; Rajasekharan, M. V.; Hureau, C.; Riviere, E.; Cano, J.; Girerd, J.-J. *Inorg. Chem*. **200**3, *42*, 180.

14. (a) Mabad, B.; Luneau, D.; Theil, S.; Dahan, F.; Sarariault, J. M.; Tuchagues, J. P. *J. Inorg. Biochem.* **1991**, *43*, 373. (b) Kennedy, B. J.; Murray, K. S. *Inorg. Chem*. **1985**, *24*, 1552.

15. (a) Matsumoto, N.; Takemoto, N.; Ohyosi, A.; Okawa, H. *Bull. Chem. Soc. Jpn.* **1988**, *61*, 2984. (b) Mikuriya, M.; Yamato, Y.; Tokii, T. *Bull. Chem. Soc. Jpn.* **1992**, *65*, 1466.

16. Miyasaka, H.; Sugimoto, K.; Sugiura, K.; Ishii, T.; Yamashita, M. *Mol. Cryst. Liq. Cryst.* **2002**, *379,* 197.

17. Miyasaka, H.; Mizushima, K.; Furukawa. S.; Sugiura, K.; Ishii, T.; Yamasaka, H. *Mol. Cryst. Liq. Cryst.* **2002**, *379*, 171.

18. Sato, Y.; Miyasaka, H.; Matsumoto, N.; Okawa, H. *Inorg. Chim. Acta* **1996**, *247*, 57.

19. Miyasaka, H.; Saitoh, A.; Abe, S. *Coord. Chem. Rev.* **2007**, *251*, 2622.

20. Reddy, K. R.; Rajasekharan, M. V.; Tuchagues, J.-P. *Inorg. Chem.* **1998**, *37*, 5978.

21. Nastase, S.; Tuna, F.; Maxim, C.; Muryn, C. A.; Avarvari, N.; Winpenny, R. E. P.; Andruh, M. *Cryst. Growth Des.* **2007**, *7*, 1825.

22. Pascal, P. *Ann. Chim. Phys*. **1910**, *19*, 5.

23. Chandramouli, G. V. R.; Balagopalakrishna, C.; Rajasekharan, M. V.; Manoharan, P. T. *Comput. Chem.* **1996**, *20*, 353.

24. O'Connor, C. J. *Prog. Inorg. Chem.* **1982***, 29*, 203.

25. Garge, P.; Chikate, R.; Padhye, S.; Savariault, J.-M.; de Loth, P.; Tuchagues, J.-P. *Inorg. Chem*. **1990**, *29*, 3315.

26. James, F.; Roos, M. "*MINUIT Program*, a System for Function Minimization and Analysis of the Parameters Errors and Correlations"; *Comput. Phys. Commun.*, **1975**, *10*, 345.

27. SAINTPLUS, Bruker AXS Inc., Madison, Wisconsin, USA, 2003.

28. Sheldrick, G. M. SADABS, Program for Empirical Absorption Correction, University of Gottingen, Gottingen, Germany **1996**.

29. Sheldrick, G. M. SHELX-97, Programs for Crystal Structure Analysis, University of Gottingen, Gottingen, Germany **1997**.

30. Nakamoto, K. *Infrared and Raman Spectra of Inorganic and coordination Compounds*; 3 ed.; John Wiley & Sons, Inc.: New York, 1997, pp 270.

31. Ginsberg, A. P.; Lines, M. E. *Inorg. Chem.* **1972**, *11*, 2289.

32. Hunter, C. A. *Chem. Soc. Rev.* **1994**, 101.

33. Nishio, M. CrystEngComm **2004**, *6*, 130.